Enhancing metal-insulator-insulator-metal tunnel diodes via defect enhanced direct tunneling

Citation	Alimardani, N., & Conley Jr, J. F. (2014). Enhancing metal-insulator-insulator-metal tunnel diodes via defect enhanced direct tunneling. Applied Physics Letters, 105(8), 082902. doi:10.1063/1.4893735
DOI	10.1063/1.4893735
Publisher	American Institute of Physics Publishing
Version	Version of Record
Terms of Use	http://cdss.library.oregonstate.edu/sa-termsofuse

Enhancing metal-insulator-insulator-metal tunnel diodes via defect enhanced direct tunneling

Nasir Alimardani[a] and John F. Conley, Jr.[b]
School of Electrical Engineering and Computer Science, Oregon State University, Corvallis, Oregon 97331, USA

(Received 6 June 2014; accepted 11 August 2014; published online 25 August 2014)

Metal-insulator-insulator-metal tunnel diodes with dissimilar work function electrodes and nanolaminate Al_2O_3-Ta_2O_5 bilayer tunnel barriers deposited by atomic layer deposition are investigated. This combination of high and low electron affinity insulators, each with different dominant conduction mechanisms (tunneling and Frenkel-Poole emission), results in improved low voltage asymmetry and non-linearity of current versus voltage behavior. These improvements are due to defect enhanced direct tunneling in which electrons transport across the Ta_2O_5 via defect based conduction before tunneling directly through the Al_2O_3, effectively narrowing the tunnel barrier. Conduction through the device is dominated by tunneling, and operation is relatively insensitive to temperature. © *2014 AIP Publishing LLC*. [http://dx.doi.org/10.1063/1.4893735]

Metal-insulator-metal (MIM) devices are of interest for hot electron transistors;[1,2] high speed diodes for rectenna based infrared (IR) energy harvesting,[3,4] IR detectors,[5] and thermal imaging;[6] selector diodes for resistive random access memory (RRAM);[7,8] tunneling cathodes;[9–11] and large area macroelectronics.[12,13] Figures of merit for MIM diodes include the asymmetry, nonlinearity, and turn-on voltage (V_{ON}). Rectification performance in MIM diodes is generally limited by the work function difference ($\Delta\Phi_M$) that can be achieved between the metal electrodes,[14] the barrier heights at either interface, and the mechanism of charge transport through the insulator.[15] The choice of insulator is critical. Wide band-gap (E_G) oxide insulators are limited by high V_{ON}.[15–17] Narrow E_G insulators such as Ta_2O_5 and Nb_2O_5 are thus attractive because small metal-insulator barrier heights allow for low V_{ON}. For stable, temperature insensitive, high speed operation, conduction through the insulator should be dominated by tunneling. However, because conduction in these materials is dominated by emission mechanisms rather than tunneling, devices based on single layers of either Ta_2O_5 or Nb_2O_5 may not be suitable for stable high speed rectification.[18]

Another approach to improving asymmetry is the use of nanolaminate insulator heterojunctions.[19,20] The idea is to pair up insulators with different E_G and electron affinity (χ) to form metal-insulator-insulator-metal (MIIM) diodes with highly asymmetric tunnel barriers.[4,21–23] Recently, we demonstrated that a nanolaminate pair of Al_2O_3 and HfO_2, combined with dissimilar work function electrodes, formed MIIM diodes with enhanced performance over single layer MIM diodes.[23] We showed that the enhancements in asymmetry were due to "step tunneling," (ST) a situation in which an electron may tunnel directly through only the larger E_G insulator instead of both. Simulations suggest that replacing the HfO_2 insulator with an even larger χ insulator such as Ta_2O_5 should result in improved low voltage asymmetry.

In this work, we investigate MIIM devices with nanolaminate bilayers of Al_2O_3 and Ta_2O_5. Al_2O_3 is a wide E_G/low χ insulator and is dominated by tunneling.[15] Ta_2O_5 is a narrow E_G/high χ insulator dominated by thermal emission based conduction.[18] Both insulators are deposited via atomic layer deposition (ALD) on an ultrasmooth amorphous metal bottom electrode. The current vs. voltage (I-V) characteristics, asymmetry, and non-linearity are investigated as a function of temperature and compared with simulations. Despite the dominance of emission based conduction in Ta_2O_5, conduction in the overall MIIM device is dominated by tunneling. We find that diode performance is enhanced by a mechanism we term "defect enhanced direct tunneling."

Devices were fabricated on Si with 100 nm of insulating SiO_2, atomically smooth (~0.3 nm RMS) ZrCuAlNi (ZCAN) amorphous metal bottom electrodes, and Al top electrodes; details reported elsewhere.[23–25] Thin insulator tunnel barriers were deposited via ALD in a Picosun SUNALE R-150B at a temperature of 250 °C using deionized water as the oxidant, tantalum ethoxide for Ta_2O_5, and trimethylaluminum for Al_2O_3. Total insulator stack thicknesses of 10 nm and 5 nm were investigated. In order to avoid the possibility of crystallization of either the ALD insulators or the electrodes, all devices are studied as-deposited, without any annealing treatments.

The thicknesses of insulator films deposited on Si were measured using a J.A. Woollam WVASE32 spectroscopic ellipsometer. I-V measurements were performed on a probe station in a dark box using an Agilent 4156C semiconductor parameter analyzer and a Temptronic gold plated ThermoChuck with the ZCAN electrode at ground and with bias applied to the Al gate. I-V curves were swept from zero bias to either the maximum positive or negative bias. V_{ON} as defined as the voltage at which current begins to increase exponentially with voltage. I-V asymmetry, η_{asym}, is defined as negative current divided by positive current $|I_-/I_+|$, so that $\eta_{asym} = 1$ indicates symmetric operation. Non-linearity, f_{NL}, is defined as $(dI/dV)/(I/V)$. Band diagrams were simulated[26] using $\chi = 1.4$ eV, $E_G = 6.4$ eV, and $\kappa = 7.6$ for Al_2O_3; $\chi = 2.25$ eV, $E_G = 5.6$ eV, and $\kappa = 18$ for HfO_2; and

[a]Now at ON Semiconductor, Gresham, Oregon 97030, USA.
[b]Author to whom correspondence should be addressed. Electronic mail: jconley@eecs.oregonstate.edu

$\chi = 3.2$ eV, $E_G = 4.4$ eV, and $\kappa = 24$ for Ta_2O_5; $\Phi_{ZCAN} = 4.8$ eV and $\Delta\Phi = \Phi_{ZCAN} - \Phi_{Al} = 0.6$ eV.[23] E_G values are based on reflective electron energy loss spectroscopy.[15] χ values are taken from the literature.[27–29] Relative dielectric constants (κ) are calculated from capacitance vs. voltage measurements.

Shown in Fig. 1 are simulated energy band diagrams of ZCAN/HfO_2/Al_2O_3/Al and ZCAN/Ta_2O_5/Al_2O_3/Al MIIM diodes for which the individual insulator layers are of equal thickness. Assuming that conduction in all insulators is dominated by tunneling, replacing the HfO_2 layer with a larger electron affinity (and higher dielectric constant) Ta_2O_5 layer should result in ST occurring at a lower V_{ON}. The simulated band diagrams in Fig. 1 indicate that the onset of ST in the (b) ZCAN/Ta_2O_5/Al_2O_3/Al stack occurs at $V_{ON} \sim -2$ V, much lower than $V_{ON} \sim -3.4$ V for the (a) ZCAN/HfO_2/Al_2O_3/Al stack. The reduction in predicted V_{ON} is due to the larger conduction band offset between Al_2O_3 and Ta_2O_5 as well as the increased relative voltage drop across the Al_2O_3 part of the capacitive voltage divider.

Shown in Fig. 2 are log current density (J) vs. V, η_{asym} vs. V, and f_{NL} vs. V plots for MIIM diodes made with Al_2O_3/Ta_2O_5 insulator stacks having a total thickness of either 5 nm or 10 nm with the same thickness for each layer (2.5 nm/2.5 nm and 5 nm/5 nm). Single insulator MIM diodes with 5 nm or 10 nm thick layers of either Al_2O_3 or Ta_2O_5 are included for comparison. Both the (c) 10 nm and (d) 5 nm thick ZCAN/Al_2O_3/Ta_2O_5/Al devices (green curves) show improved low voltage asymmetry over both single layer MIM diodes.

Plots of η_{asym} vs. V for the 5 nm thick insulator stack ZCAN/Al_2O_3/Ta_2O_5/Al MIIM diodes are compared in Fig. 3 with the 5 nm thick insulator stack ZCAN/HfO_2/Al_2O_3/Al MIIM diodes from Ref. 23 as well as ZCAN/Al_2O_3/Al MIM diodes with various Al_2O_3 thicknesses to less than 1 nm (12 ALD cycles). It is seen in Fig. 3 that decreasing Al_2O_3

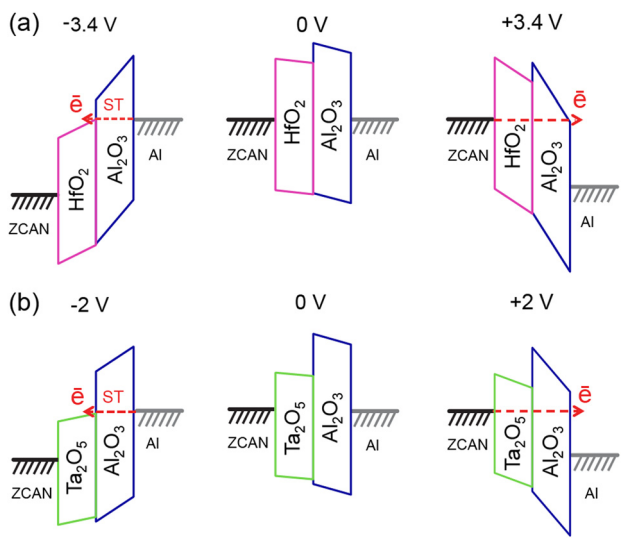

FIG. 1. Simulated energy band diagrams of (a) ZCAN/HfO_2/Al_2O_3/Al and (b) ZCAN/Ta_2O_5/Al_2O_3/Al MIIM diodes for individual insulator layers of equal thickness. In all band diagrams, the ZCAN electrode is grounded and voltage is applied to the Al electrode. Shown for both stacks are the onset of step tunneling (ST) (left), equilibrium (center), and direct tunneling through both insulators (right).

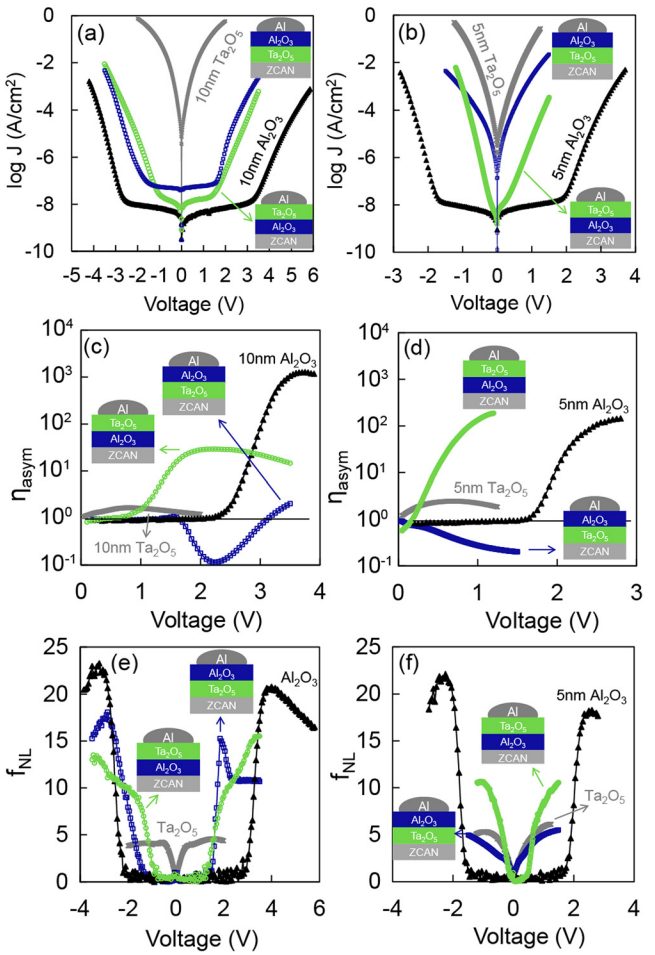

FIG. 2. Plots of log (J) vs. V, η_{asym} vs. V, and f_{NL} vs. V for single layer MIM and bilayer MIIM diodes made with Ta_2O_5 and Al_2O_3. In (a), (c), and (e), the total insulator thickness is 10 nm. In (b), (d), and (f), the total insulator thickness is 5 nm.

thickness in Al_2O_3 MIM diodes can improve low voltage asymmetry but the asymmetric response deteriorates and η_{max} shrinks because direct tunneling (DT) dominates over Fowler-Nordheim tunneling. The ST enhanced ZCAN/HfO_2/Al_2O_3/Al MIIM diodes from previous work[23] show superior low voltage asymmetry and η_{max} in comparison to similar

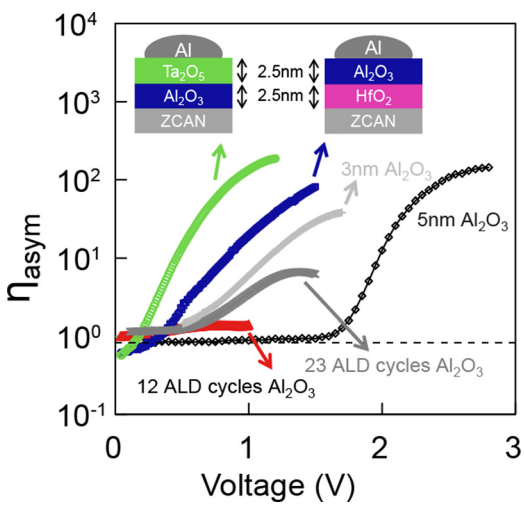

FIG. 3. Plots of η_{asym} vs. V showing (i) various Al_2O_3 thickness MIM diodes and (ii) 5 nm thick ZCAN/Al_2O_3/Ta_2O_5/Al MIIM diodes, all from this work, along with (iii) 5 nm thick ZCAN/HfO_2/Al_2O_3/Al MIIM diodes from Ref. 23.

total thickness MIM diodes ($\eta_{max.} = 82$ at 1.5 V for a 5 nm thick bilayer). The ZCAN/Al_2O_3/Ta_2O_5/Al diodes (green curve) from this work are even better, showing the best low bias asymmetry and the smallest V_{ON} (down to 0.2 V) of all the devices.

At first glance, the results in Figs. 2 and 3 seem to confirm the predictions that replacing HfO_2 with Ta_2O_5 should improve performance. However, that whereas the band diagrams in Fig. 1(b) predict $\eta_{asym} > 1$ for the ZCAN/Ta_2O_5/Al_2O_3/Al devices, $\eta_{asym} < 1$ is shown by the blue curves in Figs. 2(c) and 2(d). Likewise, the reverse stack orientation ZCAN/Al_2O_3/Ta_2O_5/Al devices (green curves in Figs. 2(c) and 2(d)) show $\eta_{asym} > 1$, instead of the expected $\eta_{asym} < 1$. This unexpected asymmetry can be explained by considering the dominant conduction mechanisms in each of the insulators. We have shown previously that while transport in the Al_2O_3 films is dominated by tunneling,[15] the Ta_2O_5 films are dominated by Frenkel-Poole emission (FPE).[18] Thus, the step-tunneling model, which assumes tunneling dominated conduction in both insulators, may not be adequate to explain the electrical behavior of the Al_2O_3-Ta_2O_5 diodes. Energy band diagrams shown in Fig. 4 depict operation of the ZCAN/Al_2O_3/Ta_2O_5/Al and ZCAN/Ta_2O_5/Al_2O_3/Al devices for which the individual insulator layers are of equal thickness. Consider first the ZCAN/Al_2O_3/Ta_2O_5/Al diode under negative applied bias, shown in Fig. 4(b). Once the Ta_2O_5 bands are downward sloped from right to left, electrons leaving the Al electrode first transport easily through the Ta_2O_5 layer via FPE before transporting across the Al_2O_3 layer via DT. Conduction through the bilayer is limited by DT through the Al_2O_3 layer, and the Ta_2O_5 layer does not appear as part of the tunneling barrier between the two electrodes. As electrons need only to tunnel across the Al_2O_3 part of the stack, an effectively decreased tunneling distance results. We will refer to this situation as *defect enhanced direct tunneling* (DEDT), due to the contributions of defects in Ta_2O_5 layer in enhancing DT through the adjacent Al_2O_3 layer. Next, consider the injection of electrons from the ZCAN electrode under a positive applied bias. As they first encounter the Al_2O_3 barrier, prior to the onset of ST, electrons must tunnel through both the Al_2O_3 and Ta_2O_5 layers. Conduction is thus initially greater for negative bias than for positive bias, resulting in $\eta_{asym} > 1$. Note that for both polarities, conduction is limited by tunneling.

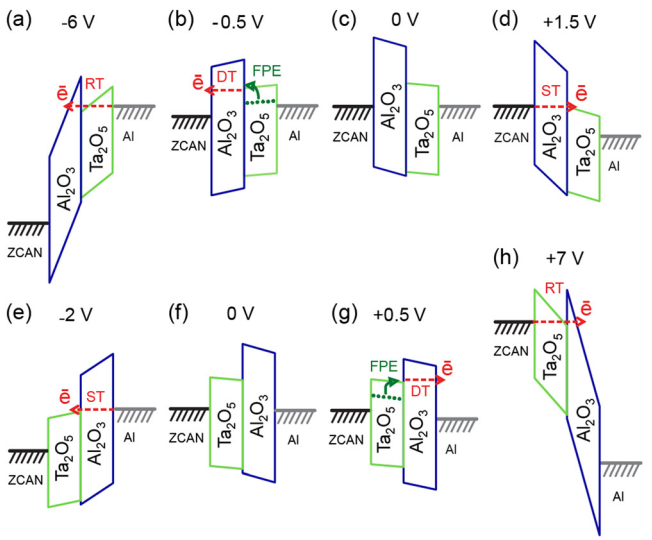

FIG. 4. Energy band diagrams of ZCAN/Al_2O_3/Ta_2O_5/Al MIIM diodes with individual insulator layers of equal thickness illustrating (a) resonant tunneling (RT), (b) defect enhanced direct tunneling, (c) equilibrium, and (d) the onset of ST. Also shown are band diagrams for ZCAN/Ta_2O_5/Al_2O_3/Al MIIM diodes illustrating (e) the onset of ST, (f) equilibrium, (g) defect enhanced direct tunneling, and (h) RT.

A similar situation is observed for the ZCAN/Ta_2O_5/Al_2O_3/Al devices. In Fig. 4(g), electrons leaving the ZCAN electrode under positive bias transport easily across the Ta_2O_5 layer via FPE before transporting across the Al_2O_3 layer via DT. Electrons leaving the Al electrode under negative bias, prior to the onset of ST, must tunnel through both barriers. Once again, conduction is initially greater for the polarity at which DEDT occurs, resulting in $\eta_{asym} < 1$.

Shown in Figs. 2(e) and 2(f) are f_{NL} plots for the same devices. It is seen that the f_{NL} changes are consistent with change in the asymmetric response. The ZCAN/Al_2O_3/Ta_2O_5/Al diodes with superior low-voltage asymmetry also demonstrate superior non-linearity, up to $f_{NL} = 10$ in voltage regimes smaller than ± 1 V.

There are four competing mechanisms for inducing asymmetry in tunnel diodes:

(i) Dissimilar metal electrodes: As seen in Figs. 4(c) and 4(f), the use of dissimilar work function metal electrodes will induce a built-in voltage drop across the insulator stack. Electron transport from the smaller Φ_M (smaller barrier height) electrode is enhanced. Asymmetry is induced in proportion to (and is thus limited by) $\Delta\Phi_M$.

(ii) Step tunneling: When low χ (wide E_G) insulators are matched with higher χ (narrower E_G) insulators and both insulators are dominated by tunneling, low voltage range conduction may be enhanced for electron injection from the electrode adjacent to the low χ insulator by the onset of DT through only the low χ insulator, as shown in Fig. 1, as well as Figs. 4(d) and 4(e).

(iii) Defect enhanced direct tunneling: If the dominant conduction mechanism through the low χ insulator is tunneling and defect enhanced (FPE or trap assisted tunneling (TAT)) dominates in the high χ insulator, then low voltage regime conduction may be enhanced for electron injection from the electrode adjacent to the high χ insulator. Transport across the high χ insulator proceeds via FPE or TAT, so that DT may occur through only the low χ insulator, effectively decreasing the tunnel distance for one polarity. This mechanism is illustrated in Figs. 4(b) and 4(g).

(iv) Resonant tunneling (RT): When conduction through both insulators layers is dominated by tunneling and the applied bias is large enough so that quantized energy levels between the insulators are formed in line with the Fermi level of one of the electrodes, conduction may be enhanced. As shown in Figs. 4(a) and 4(h), the voltage required for the onset of RT is typically large and simulations show it generally exceeds the breakdown strength of the insulator stack. RT is thus not relevant to the operation of the devices in this work.

TABLE I. Summary of mechanisms causing asymmetry in MIM and MIIM diodes made with ZCAN bottom electrodes and Al top electrodes. For the MIIM diodes, individual insulator layers of equal thickness are assumed. N/A = not applicable.

Asymmetry mechanism	$\Delta\Phi_M$	Step tunneling	Defect enhanced direct tunneling	Resonant tunneling
ZCAN/Al_2O_3/Al	$\eta_{asym} > 1$	N/A	N/A	N/A
Ta_2O_5	$\eta_{asym} > 1$	N/A	N/A	N/A
Al_2O_3/Ta_2O_5	$\eta_{asym} > 1$	$\eta_{asym} < 1$ ($V_{onset} \gtrsim 1.5$ V)	$\eta_{asym} > 1$	N/A
Ta_2O_5/Al_2O_3	$\eta_{asym} > 1$	$\eta_{asym} > 1$ ($V_{onset} \lesssim -2$ V)	$\eta_{asym} < 1$	N/A
Al_2O_3/HfO_2	$\eta_{asym} > 1$	$\eta_{asym} < 1$ ($V_{onset} \gtrsim 3$ V)	N/A	N/A ($V_{onset} \lesssim -8$ V)
HfO_2/Al_2O_3	$\eta_{asym} > 1$	$\eta_{asym} > 1$ ($V_{onset} \lesssim -3.4$ V)	N/A	N/A ($V_{onset} \gtrsim 5.2$ V)

It is seen in Figs. 2(c) and 2(d) that stacks starting with Al_2O_3 on the ZCAN bottom electrode (green curves) exhibit larger magnitude asymmetry than the stacks starting with Ta_2O_5 on the ZCAN (blue curves). The first three asymmetry mechanisms described above can explain qualitatively the observed differences in η_{max}. The impact of these mechanisms on asymmetry is summarized in Table I for all devices. The $\Delta\Phi_M$ induces $\eta_{asym} > 1$ in all MIM and MIIM devices. Thus, both single layer Al_2O_3 and Ta_2O_5 devices show $\eta_{asym} > 1$. The asymmetry induced by ST and DEDT is more complex.

For the ZCAN/Al_2O_3/Ta_2O_5/Al devices, ST induces $\eta_{asym} < 1$ for $V_{appl} > 1.5$ V. DEDT induces $\eta_{asym} > 1$. In these devices, DEDT and $\Delta\Phi_M$ align to compete with ST and $\eta_{asym} > 1$ is shown in the green curves in Figs. 2(c) and 2(d). For the 10 nm thick devices, η_{asym} shows a maximum and begins to decrease as ST grows stronger. For the 5 nm devices, the diodes reach breakdown before reaching ST and thus η_{asym} does not saturate.

For the ZCAN/Ta_2O_5/Al_2O_3/Al devices, ST induces $\eta_{asym} > 1$ for $V_{appl} < -2$ V. DEDT induces $\eta_{asym} < 1$. For these devices, DEDT must compete against both ST and $\Delta\Phi_M$. Thus η_{max} for this device is not as great as for the opposite orientation of the insulator layers. Shown in the blue curves in Figs. 2(c) and 2(d), DEDT initially dominates and $\eta_{asym} < 1$. In the 10 nm device, η_{asym} eventually becomes greater than one after ST turns on and begins to dominate. For the 5 nm devices, the diodes reach breakdown before reaching ST and thus the reversal in η_{asym} does not occur.

The DT process through the Al_2O_3 layer, to first order, operates independent of temperature. FPE conduction through the Ta_2O_5 layer, however, is expected to be exponentially sensitive to temperature. In the bilayer Al_2O_3/Ta_2O_5 MIIM devices, these transport mechanisms operate in series. The exponential rise of current above the knees in the log (J) vs. V plots in Fig. 2(a) and the discussion of the band diagrams in Fig. 4 suggest that conduction in bilayer Al_2O_3/Ta_2O_5 devices is limited by DT through the Al_2O_3 layer. Temperature insensitive operation is therefore expected, despite the participation of FPE in the Ta_2O_5 layer. Shown in Fig. 5 are plots of log (J) vs. V and η_{asym} vs. V for both stack orientations of the 5 nm thick Al_2O_3/Ta_2O_5 diodes at 300, 325, and 375 K. It is seen that operation of these devices is relatively insensitive to temperature, additional evidence that conduction in these MIIM devices is limited by DT.

We demonstrated previously that bilayer-insulator ZCAN/HfO_2/Al_2O_3/Al MIIM diodes with dissimilar work function electrodes exhibited enhanced performance over single insulator MIM diodes and that the enhancements were due to step tunneling. In this work, we show that asymmetry and V_{ON} may be further improved by pairing Al_2O_3 with Ta_2O_5, a high χ insulator dominated by FPE. The observed improvement in asymmetry, however, is not consistent with ST. Instead, the enhanced performance may be explained by DEDT, in which electrons injected from the electrode adjacent to the high χ insulator transport easily across this insulator via defect based FPE before tunneling directly through the lower χ insulator. This results in an effectively narrowed tunnel barrier for one polarity. Electrons traveling under the opposite polarity must tunnel through both insulators. Whereas ST produces the most improvement when the high χ insulator is adjacent to large Φ_M electrode,[23] in this work DEDT produces the most improvement when the low χ insulator is adjacent to large Φ_M electrode. For the 5 nm thick ZCAN/Al_2O_3/Ta_2O_5/Al diodes, $\eta_{asym} = 10$ and $f_{NL} = 6.5$ at 0.45 V, $\eta_{max} = 187$ at 1.2 V, and $f_{NL\text{-}max} = 11$ at −1.1 V was achieved. Conduction in DEDT enhanced Al_2O_3/Ta_2O_5 bilayer devices is dominated by tunneling, despite the dominance of FPE in Ta_2O_5. Operation is relatively insensitive to temperature, making these devices suitable for stable high speed operation. The MIIM architecture not only allows insulators dominated by emission based conduction to be used in temperature insensitive diodes, but actually takes advantage of defect conduction to improve asymmetry

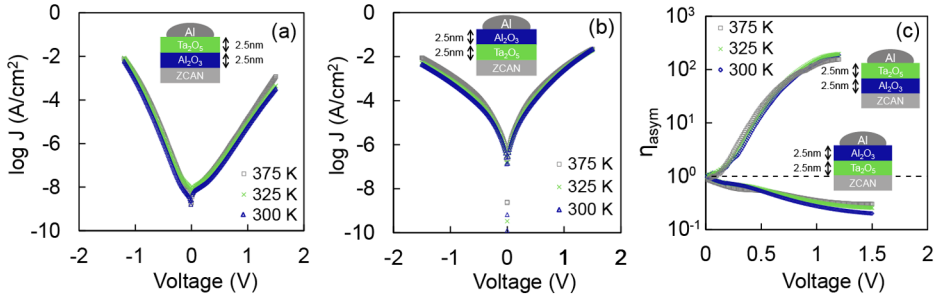

FIG. 5. Plots of log J vs. V for 5 nm thick insulator stack (a) ZCAN/Al_2O_3/Ta_2O_5/Al and (b) ZCAN/Ta_2O_5/Al_2O_3/Al MIIM diodes at temperatures of 300, 325, and 375 K. (c) Plot of η_{asym} vs. V for both stack orientations.

through DEDT. Optimization of the bilayer stack and the relative thicknesses of the insulator layers (equal thicknesses were used in this work) will enable further improvements in performance.

This work was supported in part by grants from the National Science Foundation through DMR-0805372 with matching support from the Oregon Nanoscience and Microtechnologies Institute (ONAMI). The authors thank Professor J. F. Wager and John McGlone of OSU for ZCAN films, C. Tasker of the OSU Materials Synthesis and Characterization (MASC) Facility for equipment support.

[1]S. Vaziri, G. Lupina, C. Henkel, A. D. Smith, M. Östling, J. Dabrowski, G. Lippert, W. Mehr, and M. C. Lemme, Nano Lett. **13**(4), 1435 (2013).
[2]C. Zeng, E. B. Song, M. Wang, S. Lee, C. M. Torres, Jr., J. Tang, B. H. Weiller, and K. L. Wang, Nano Lett. **13**(6), 2370 (2013).
[3]M. N. Gadalla, M. Abdel-Rahman, and A. Shamim, Sci. Rep. **4**, 4270 (2014).
[4]*Rectenna Solar Cells*, edited by G. M. Moddel and S. Grover (Springer, New York, 2013).
[5]P. C. D. Hobbs, R. B. Laibowitz, F. R. Libsch, N. C. LaBianca, and P. P. Chiniwalla, Opt. Express **15**(25), 16376 (2007).
[6]E. C. Kinzel, R. L. Brown, J. C. Ginn, B. A. Lail, B. A. Slovick, and G. D. Boreman, Microwave Opt. Technol. Lett. **55**, 489 (2013).
[7]B. Govoreanu, C. Adelmann, A. Redolfi, L. Zhang, S. Clima, and M. Jurczak, IEEE Electron Device Lett. **35**(1), 63 (2014).
[8]R. D. Clark, Materials **7**, 2913–2944 (2014).
[9]T. W. Hickmott, J. Appl. Phys. **108**, 093703 (2010).
[10]T. W. Hickmott, J. Appl. Phys. **114**, 233702 (2013).
[11]M. Suzuki, M. Sagawa, T. Kusunoki, E. Nishimura, M. Ikeda, and K. Tsuji, IEEE Trans. Electron Devices **59**, 2256 (2012).
[12]W. den Boer, *Active Matrix Liquid Crystal Displays* (Elsevier, Amsterdam, 2005), pp. 43–47.
[13]R. H. Reuss, B. R. Chalamala, A. Moussessian, M. G. Kane, A. Kumar, D. C. Zhang, J. A. Rogers, M. Hatalis, D. Temple, G. Moddel *et al*., Proc. IEEE **93**(7), 1239 (2005).
[14]J. G. Simmons, J. Phys. D: Appl. Phys. **4**, 613 (1971).
[15]N. Alimardani, S. W. King, B. L. French, C. Tan, B. P. Lampert, and J. F. Conley, Jr., J. Appl. Phys. **116**, 024508 (2014).
[16]S. M. Sze and K. K. Ng, *Physics of Semiconductor Devices*, 3rd Ed. (Wiley-Interscience, Hoboken, NJ, 2007).
[17]J. Robertson, J. Vac. Sci. Technol. B **18**, 1785 (2000).
[18]N. Alimardani, J. M. McGlone, J. F. Wager, and J. F. Conley, Jr., J. Vac. Sci. Technol. A **32**(1), 01A122 (2014).
[19]H. Kroemer, Phys. Scr. **T68**, 10 (1996).
[20]P. A. Schulz and C. E. T. Gonçalves da Silva, Appl. Phys. Lett. **52**(12), 960 (1988).
[21]M. Di Ventra, G. Papa, C. Coluzza, A. Baldereschi, and P. A. Schulz, J. Appl. Phys. **80**(7), 4174 (1996).
[22]P. Maraghechi, A. Foroughi-Abari, K. Cadien, and A. Y. Elezzabi, Appl. Phys. Lett. **99**, 253503 (2011).
[23]N. Alimardani and J. F. Conley, Jr., Appl. Phys. Lett. **102**, 143501 (2013).
[24]E. E. Cowell III, N. Alimardani, C. C. Knutson, J. F. Conley, Jr., D. A. Keszler, B. J. Gibbons, and J. F. Wager, Adv. Mater. **23**(1), 74 (2011).
[25]N. Alimardani, E. W. Cowell III, J. F. Wager, J. F. Conley, Jr., D. R. Evans, M. Chin, S. J. Kilpatrick, and M. Dubey, J. Vac. Sci. Technol. A **30**(1), 01A113 (2012).
[26]R. G. Southwick III, A. Sup, A. Jain, and W. B. Knowlton, IEEE Trans. Device Mater. Reliab. **11**(2), 236 (2011).
[27]S. Swaminathan, Y. Sun, P. Pianetta, and P. C. McIntyre, J. Appl. Phys. **110**, 094105 (2011).
[28]S. Monaghan, P. K. Hurley, K. Cherkaoui, M. A. Negara, and A. Schenk, Solid-State Electron. **53**(4), 438 (2009).
[29]C.-H. Cheng and J. Y.-M. Lee, Appl. Phys. Lett. **91**, 192903 (2007).